Biochimica et Biophysica Acta 1818 (2012) 1613–1624

Contents lists available at SciVerse ScienceDirect

Biochimica et Biophysica Acta

journal homepage: www.elsevier.com/locate/bbamem

Structure, activity and interactions of the cysteine deleted analog of tachyplesin-1 with lipopolysaccharide micelle: Mechanistic insights into outer-membrane permeabilization and endotoxin neutralization

Rathi Saravanan, Harini Mohanram, Mangesh Joshi, Prerna N. Domadia, Jaume Torres, Christiane Ruedl, Surajit Bhattacharjya *

School of Biological Sciences, Division of Structural and Computational Biology, Nanyang Technological University, Singapore 637551, Singapore

ARTICLE INFO

Article history:
Received 31 January 2012
Received in revised form 14 March 2012
Accepted 16 March 2012
Available online 23 March 2012

Keywords:
Antimicrobial peptide
Lipopolysaccharide
NMR
Structure
Endotoxin
STD-NMR

ABSTRACT

Tachyplesin-1, a disulfide stabilized β-hairpin antimicrobial peptide, can be found at the hemocytes of horse shoe crab *Tachypleus tridentatus*. A cysteine deleted linear analog of tachyplesin-1 or CDT (KWFRVYRGIYRRR-NH_2) contains a broad spectrum of bactericidal activity with a reduced hemolytic property. The bactericidal activity of CDT stems from selective interactions with the negatively charged lipids including LPS. In this work, CDT–LPS interactions were investigated using NMR spectroscopy, optical spectroscopy and functional assays. We found that CDT neutralized LPS and disrupted permeability barrier of the outer membrane. Zeta potential and ITC studies demonstrated charge compensation and hydrophobic interactions of CDT with the LPS-outer membrane, respectively. Secondary structure of the peptide was probed by CD and FT-IR experiments indicating β-strands and/or β-turn conformations in the LPS micelle. An ensemble of structures, determined in LPS micelle by NMR, revealed a β-hairpin like topology of the CDT peptide that was typified by an extended cationic surface and a relatively shorter segment of hydrophobic region. Interestingly, at the non-polar face, residue R11 was found to be in a close proximity to the indole ring of W2, suggesting a cation–π type interactions. Further, saturation transfer difference (STD) NMR studies established intimate contacts among the aromatic and cationic residues of CDT with the LPS micelle. Fluorescence and dynamic light scattering experiments demonstrated that CDT imparted structural destabilization to the aggregated states of LPS. Collectively, atomic resolution structure and interactions of CDT with the outer membrane-LPS could be exploited for developing potent broad spectrum antimicrobial and anti-sepsis agents.

1. Introduction

The emergence of drug-resistant bacteria has caused a major challenge to the human health care [1,2]. There are now a number of bacteria, termed as multi drug resistant strains or superbugs, with protection against a number of conventional antibiotics [3–5]. Among these superbugs, as comprehended, the Gram-negative ones e.g. *Pseudomonas aeruginosa*, *Acinetobacter baumannii*, and *Klebsiella pneumoniae* thought to be a major threat due to the deficiency of the active drug candidates in the pipeline [5]. Therefore, novel antibiotics with different modes of actions are highly desirable to combat infectious diseases. Cationic antimicrobial peptides (AMPs) are an integral component of the innate immune system. AMPs serve as the first line of defense with a broad spectrum of activity against bacteria, viruses and fungi [6–9]. The evolutionary preserved AMPs have been recognized as a promising lead for the development of new antibiotics [6–9]. In humans, AMPs are involved for the probable stimulation and modulation of adaptive immunity [10,11]. As a mode of action, most of the AMPs disrupt the integrity of bacterial membranes [12–14]. The amphipathic sequence features, typified by the preponderance of cationic and hydrophobic amino acids, of AMPs facilitate membrano-lytic activity toward microorganisms [12–14]. The disruption of cytosolic membrane by AMPs, causing cell lysis, may occur following one or several mechanisms e.g. barrel stave, toroidal pore, carpeting sinking raft and lipid clustering [15–18]. Thus, structural or SAR studies of AMPs are largely preformed with model membranes consisted of negatively charged phospholipids plausibly mimicking the plasma membrane of bacteria [15–18]. It may be noted that while a variety of biophysical methods has been utilized to understand interactions of AMPs with model lipid membranes, the use of NMR techniques provided atomic-resolution insights in terms of structure, membrane orientation and mechanisms [18,19].

Abbreviations: AMPs, antimicrobial peptides; CDT, cysteine deleted analog of tachyplesin-1; LPS, lipopolysaccharide; NMR, nuclear magnetic resonance; Tr-NOE, transferred nuclear Overhauser effect; NOESY, nuclear Overhauser effect spectroscopy; TOCSY, total correlation spectroscopy; CD, circular dichroism; NOE, nuclear Overhauser enhancement; STD-NMR, saturation transfer difference NMR

* Corresponding author at: 60 Nanyang Drive, 637551, Singapore. Fax: +65 6791 3856.
E-mail address: surajit@ntu.edu.sg (S. Bhattacharjya).

0005-2736/$ – see front matter © 2012 Elsevier B.V. All rights reserved.
doi:10.1016/j.bbamem.2012.03.015

The outer membrane of Gram-negative organisms establishes an efficient permeability barrier for antibiotics, AMPs and host defense proteins [19–22]. A higher lethal concentration of AMPs is often necessary to prevent growth of Gram-negative organisms as compared to Gram-positive counterparts [23,24]. Some AMPs are known to be quite ineffective against Gram-negative strains [23,24]. As observed, in the context of LPS these AMPs undergo self-association preventing their translocation through the outer membrane [24–26]. Therefore, AMPs need to disrupt LPS mediated barrier of the outer membrane in order to achieve the broad spectrum activity. Chemically, LPS consists of three different segments, a distally located variable polysaccharide or O-antigen domain, a relatively conserved hexa-acylated lipid A moiety and an oligosaccharide domain covalently linking the lipid A and O-antigen domains. Consequently, atomic-resolution structures and interactions of AMPs in LPS lipids are vital to realize the mechanism of action and for the further development of highly active peptide based antibiotics [27–32]. Moreover, LPS, as termed endotoxin, is the causative agent of fatal septic shock syndromes in human [33,34]. Thus, AMPs with LPS binding and neutralizing ability may endow with scaffolds for the generation of anti-endotoxic drugs [27,35,36].

Tachyplesin-1 or TP-1 (KWCFRVCYRGICYRRCR-NH_2) is a well characterized, structurally and mechanistically, AMP from the hemocyte of horse shoe crab [37–39]. TP-1 has a broad spectrum of antimicrobial activity against several strains of Gram-negative and Gram-positive bacteria, fungi and viruses [40,41]. The antimicrobial activity of TP-1 appears to stem from the ability of the peptide to disorganize bacterial cell membranes [37–39]. NMR studies demonstrated that TP-1 adopts β-hairpin structure in solution and also in lipid micelles and bilayers [38,42,43]. The antiparallel β-strands of β-hairpin structure of TP-1 are constrained by the disulfide bridges between residues Cys3–Cys15 and Cys7–Cys12 [37,38]. Replacement of disulfide bonds with various amino acids has yielded important insight toward structure–activity relationship for β-hairpin or β-sheet AMPs including TP-1 [44–47]. However, the consequences, in terms of activity and structures, of a complete deletion of Cys residues from the amino acid sequences of AMPs had been less frequently examined. In this regard, a shorter analog of TP-1, 13-residue long, termed CDT, whereby all of the four Cys residues were deleted from the primary structure of AMP, was investigated for antibacterial activity, red blood cell lysis and liposome leakage and vesicle binding [48]. CDT demonstrated a marked inhibition of growth of Gram negative and Gram positive bacterial strains akin to TP-1. The MIC (minimum inhibitory concentration) values of CDT were even found to be lower against *Escherichia coli* and *Listeria monocytogenes* in comparison to the native TP-1 peptide. In addition, CDT did not cause any measurable hemolysis of erythrocytes at a concentration as high as 200 μg/mL. Using a variety of biophysical methods including solid state NMR studies, Ramamoorthy and coworkers demonstrated selective interactions of CDT with the negatively charged lipid vesicles e.g. POPE/POPG, POPC/POPG and POPC/LPS [48]. Based on the solid state ^{31}P NMR experiments with various lipid bilayers (POPC, POPC/POPG), it was proposed that CDT may destabilize head group packing of the lipid bilayers as a probable mode for bacterial cell lysis. However, atomic resolution structures of CDT in any of these lipid environments, in particular with the LPS-outer membrane, are yet to be known. To gain insights into the outer membrane permeabilization and endotoxin neutralization, in this work, we have characterized atomic resolution structure and interactions of CDT in LPS micelle by use of NMR spectroscopy, ITC, dynamic light scattering and optical spectroscopy methods.

2. Materials and methods

2.1. Peptide, lipids and chemicals

LPS from *E. coli* 0111:B4, fluorescein isothiocyanate (FITC) conjugated LPS from *E. coli* 055:B5 and 1-N-phenylnaph-thylamine (NPN) were purchased from Sigma-Aldrich (St. Louis, MO). POPC (1-palmitoyl-2-oleoyl-sn-glycero-3-phosphatidylcholine) was obtained from Avanti Polar Lipids™. CDT peptide was synthesized commercially by GL-Biochem (Shanghai, China) and was further purified by the reverse-phase HPLC, Waters™, using a C_{18} column (300 Å pore size, 5 μm particle size) with a linear gradient of acetonitrile/water mixture. The molecular weight of the peptide was confirmed by mass spectrometry.

2.2. Outer membrane permeabilization assay

Outer membrane permeabilization activity of CDT was analyzed by 1-N-phenylnaph-thylamine (NPN) dye uptake. Mid-log phase *E. coli* cells, obtained from an overnight culture, were centrifuged at 3000 *g* and resuspended in 10 mM sodium phosphate buffer to an optical density of 0.6 at 600 nm. A stock solution of NPN previously prepared in acetone was added to a final concentration of 10 μM in 500 μL of *E. coli* cells and a basal fluorescence was recorded. The NPN dye was excited at 350 nm and the increase in fluorescence intensity (emission maximum) at 410 nm as a function of increasing peptide concentrations (0.5–10 μM) was recorded. The maximal value of NPN uptake was determined after the addition of 10 μL polymyxin B sulfate (0.64 mg/mL stock). The results were presented as percentage membrane permeabilization relative to the membrane permeabilization observed for polymyxin B.

2.3. TNF-α release assay

Murine macrophage (Raw 264.7) cells were revived to confluency in IMDM medium supplemented with FCS, glutamine and penicillin: streptomycin in a 96 well micro-titer plate. A serial dilution of CDT peptide from 1 μM to 10 μM was incubated with different concentrations of LPS (1 ng/mL to 100 ng/mL) for 30 min. Peptide–LPS complex was then added to confluent macrophage cells and further incubated for 6 h. The supernatant from each well was then analyzed by conventional ELISA according to the manufacturer's instruction. The release of TNF-α was then detected spectrophotometrically at 540 nm.

2.4. Measurement of surface charge

Zeta potential studies for surface charge measurements were carried out on a Zetasizer Nano ZS (Malvern Instruments, UK) equipped with a 633 nm HeNe laser. *E. coli* cells were grown to mid-log phase from overnight grown culture and suspended in 10 mM sodium phosphate buffer, pH 6.8 to a final O.D. of 0.2. POPC:LPS (80:20 w/w) LUVs were prepared by extrusion method. *E. coli* cells or LUVs were loaded into a disposable zeta cell with gold electrode and the samples were allowed to equilibrate for 3 min at 25 °C. Measurements were made as a function of increasing concentration of CDT. A total of 5 measurements of 100 runs each were carried out for all the concentrations of peptide.

2.5. Fluorescence studies

All of the fluorescence experiments were carried out in a Cary Eclipse fluorescence spectrophotometer (Varian, Inc., Australia) equipped with a dual monochromator. Measurements were performed using a 0.1 cm path length cuvette and a band width of 5 nm for excitation and emission. Intrinsic tryptophan fluorescence spectra of CDT were recorded by titrating 5 μM peptide with increasing concentrations of *E. coli* 0111:B4 LPS. Fluorescence spectra were recorded in 10 mM sodium phosphate buffer at pH 6.0. Fluorescence quenching experiments for free and LPS micelle bound peptide were recorded by stepwise addition of (0.02–0.2 M) acrylamide either into the peptide or peptide–lipid solutions of 5 μM LPS. Quenching of fluorescence intensity at the emission maximum for the free and LPS bound forms of CDT was noted and results were analyzed

using Stern–Volmer's quenching equation $F_o/F = 1 + K_{SV}[Q]$, where F_o and F are the fluorescence intensity at the emission maximum in the absence and presence of quencher, respectively, K_{SV} is the Stern–Volmer quenching constant and [Q] is the molar concentration of acrylamide. The emission spectra, from 500 to 600 nm, of FITC conjugated LPS, in 10 mM sodium phosphate buffer, pH 6.0, were recorded with the excitation at 480 nm in samples containing 0.5 μM FITC-LPS.

2.6. Isothermal titration calorimetry (ITC) experiments

Binding affinity of CDT with LPS and thermodynamic parameters of interactions were determined using ITC experiments on a Nano-ITC calorimeter (Micro Cal Inc, Northampton, MA). CDT and LPS were separately dissolved in a 10 mM sodium phosphate buffer, pH 6.0. LPS samples were further vortexed for 10 min and sonicated for 5 min prior to use. Twenty injections, 0.4 μL each, from 550 μM stock of CDT were made into a solution of 50 μM LPS, at an interval of 4 min, with a stirring speed of 300 rpm and the heat exchange was recorded at 20 °C. The heat of dilution of the peptide alone into the buffer was subtracted from the titration data. The resulting data were integrated with Micro Cal Origin 7.0. The data was fitted with models provided in the software and analyzed to determine the association constant K_a and the enthalpy change ΔH. The Gibb's free energy change ΔG and entropy change ΔS were calculated from the fundamental thermodynamic equations: $\Delta G = -RT \ln K_a$ and $T\Delta S = (\Delta H - \Delta G)$, respectively.

2.7. Dynamic light scattering (DLS) studies

Particle size distribution of LPS micelle in the presence and absence of CDT was determined using DLS measurements, performed on a BI-200SM instrument equipped with a He–Ne laser and a BI-900 AT auto-correlation system (Brookhaven Instruments Corp., Holtsville, NY). For DLS measurement, 1 μM LPS was dissolved in a 10 mM sodium phosphate buffer, pH 6.0 and was exposed to 90° light scattering for 3 min. DLS measurements were recorded for LPS in the presence of 2 μM CDT, under similar conditions. All samples were filtered, degassed and scanned using a 1-mm path length quartz cuvette. Data were analyzed by the CONTIN method supplied with the instrument.

2.8. Circular dichroism (CD) and IR spectroscopy

Far-UV CD spectra of CDT were recorded using a Chirascan CD spectrophotometer (Applied Photophysics Ltd., UK) with a 0.1 mm path length of cuvette. CD data were collected with a spectral bandwidth of 1 nm and a time constant of 1 s. Peptide concentration in all experiments was fixed to 100 μM. 50 μM LPS was used to record secondary structural changes in the presence of lipid. Samples were prepared in 10 mM sodium phosphate buffer at pH 6.0. FTIR spectra were recorded on a Nicolet Nexus 560 spectrometer (Madison, USA) purged with N_2 and equipped with a MCT/A detector cooled with liquid nitrogen. Attenuated total reflection (ATR) spectra were measured with a 25-reflection ATR accessory from Graseby Specac (Kent, UK) and a wire grid polarizer (0.25 μM, Graseby Specac). Approximately 200 μL of a D_2O solution of LPS alone or in the presence of peptide in a 20:1 lipid/peptide molar ratio was applied onto a trapezoidal (50 mm × 2 mm × 20 mm) Ge internal reflection element (IRE). A dry, or D_2O saturated, N_2 stream flowing through the ATR compartment was used to remove bulk water (low hydration) or to fully hydrate the sample (high hydration), respectively. A total of 200 scans were collected at a resolution of 4 cm^{-1}, averaged and processed with one-point zero filling and Happ-Genzel apodization. Percentages of secondary structure were estimated by fitting the amide I region (from 1700 to 1600 cm^{-1}) after mild Fourier deconvolution. The amide I band was Fourier self-deconvolved (FSD) using a full-width at a half-height (FWHH) of 20 cm^{-1} and an enhancement factor, *k*, of 2.0.

2.9. NMR experiments and structure determination

NMR experiments were performed on a Bruker DRX 600 MHz spectrometer (Germany), equipped with a cryo-probe and pulse field gradients. NMR data processing and analysis were carried out using the programs Topspin (Bruker) and SPARKY (Goddard, T. D., and Kneller, D. G., University of California, San Francisco), respectively. A series of one dimensional ^1H NMR spectra of CDT was obtained by titrating aliquots of LPS, from a stock solution of 0.5 mM, in aqueous solution at pH 4.5 at 298 K. Two dimensional ^1H–^1H NOESY (mixing time: 150 and 200 ms) and TOCSY (mixing time: 80 ms) spectra of CDT, at 0.5 mM, in the presence of 10 μM LPS were acquired. NOESY spectra of CDT in free solution were also obtained in an aqueous solution at pH 4.5 at 298 K. Saturation transfer difference (STD) NMR experiments were carried out as described previously [49,50]. Typically, CDT (0.5 mM) was dissolved in 550 μL of D_2O and pH was adjusted to 4.5. Stock solution, 5 mg/mL, of LPS was prepared in D_2O solution at pH 4.5. All STD experiments were performed at 298 K in the presence of 10 μM LPS concentration using standard STD pulse sequences and WATERGATE 3-9-19 sequence for water suppression [49,50]. The on-resonance frequency of STD studies was fixed by acquiring a series of one-dimensional STD spectra at different on-resonances in the range of 0 to −10 ppm with an interval of 0.5 ppm. Finally, an on-resonance frequency was set to −3.5 ppm while the off-resonance frequency was fixed to 40 ppm for STD experiments. One dimensional STD NMR experiments were performed with a scan number of 1024 for a typical spectral width of 12 ppm. All STD spectra were multiplied by an exponential line broadening function of 3 Hz, prior to Fourier transformation. Two-dimensional STD-TOCSY spectra were recorded with 350 increments in t_1 and 80 transients using a MLEV-17 spin lock field of 80 ms. The relaxation delay was set to 2.1 s. Saturation transfer was achieved by using 40 selective Gaussian 270 pulses with a duration of 50 ms.

LPS-bound structure of CDT was calculated based on NOE-driven distance restraints. The upper bound of the inter proton distance was determined from the volume of NOESY cross-peaks. The lower bound of the inter proton distance was fixed to 2.0 Å. It should be noted that determination of the three-dimensional structure of the peptide was largely driven by the medium and long-range NOEs, exclusively present in the LPS bound state. The backbone dihedral angle (Φ) was varied from −30 to −120° for non-glycine residues to limit the conformational search. NMR structures of CDT were iteratively calculated from an extended polypeptide chain in 7 cycles of simulated annealing using Cyana 2.1 [51] program. The 20 lowest-energy structures without distance violations greater than 0.3 Å and no angle violations greater than 5° were accepted into the final ensemble. Structures were visualized using MOLMOL and PyMOL software. The quality of structures was determined using Procheck [52] and the Protein Structure Validation Suite [53].

3. Results

3.1. Neutralization of LPS toxicity and disruption of the LPS-outer membrane barrier by CDT

Owing to the interactions with the outer membrane of Gram-negative bacteria, AMPs may confer neutralization of the toxicity of LPS or endotoxin [19,27]. However, it may be noted that a number of AMPs despite their interactions with LPS or outer membrane are incapable of neutralizing endotoxin [27,54]. Typically, binding of endotoxin neutralizing molecules with LPS would inhibit the activation of a cell surface receptor, TLR4, causing an inhibition of the

production of tissue damaging cytokines e.g. TNF-α, IL6 and others [55]. The ability of CDT to neutralize endotoxin was examined by cytokine, TNF-α, release assays from murine macrophage RAW cells. In these experiments, macrophage cells were induced by three different concentrations, 1 ng/mL, 10 ng/mL and 100 ng/mL, of LPS either in the absence or in the presence of three different concentrations, 0.1 μM, 1 μM and 10 μM, of CDT peptide. As expected, CDT peptide was able to inhibit, in a dose-dependent manner, LPS mediated TNF-α secretion from macrophages (Fig. 1A). CDT, at a concentration of 10 μM, had caused >80% neutralization of endotoxin even for the highest concentration of LPS (100 ng/mL) (Fig. 1A). In addition, a significant inhibition of TNF-α production was seen for the lower doses, 0.1 μM and 1 μM, of CDT for LPS concentrations of 1 ng/mL and 10 ng/mL (Fig. 1A). There was >70% neutralization of endotoxin by CDT, at concentrations of 0.1 μM and 1 μM, against 1 ng/mL and 10 mg/mL LPS, respectively (Fig. 1A).

In order to exert lethal effect against Gram-negative pathogens, potent AMPs should disrupt the integrity of the outer-membrane. 1-N-phenylnaphthylamine (NPN) is a fluorescent hydrophobic dye which shows a low intensity of fluorescence emission in aqueous solution. NPN is excluded by the outer-membrane; however, a loss in the integrity of outer-membrane facilitates incorporation of NPN to the cell membranes yielding an enhanced fluorescence intensity of the probe.

We measured NPN fluorescence emission in solutions containing *E. coli* cells either in the absence or in the presence of different concentrations of CDT peptide. The emission intensity of NPN, in *E. coli* cell solutions, was also determined for 10 μM polymyxin B as a positive control. The relative emission intensity of NPN measured at different concentrations of CDT was expressed with respect to that of polymyxin B (Fig. 1B). Fig. 1B shows the relative fluorescence increase of NPN as a function of concentrations of CDT peptide. As evident, additions of CDT peptide caused a dramatic increase in the relative fluorescence intensity of NPN, indicating a permeabilization of the LPS-outer membrane. There was also a progressive blue shift in the emission maxima of NPN with increase in concentrations of CDT (Fig. 1B, inset). Thus, in the presence of CDT, NPN was able to insert into the hydrophobic environment of membranes of *E. coli* cells yielding increased fluorescence intensity and a blue shift for the emission maximum. In other words, CDT induced an efficient permeabilization of the outer-membrane of *E. coli* cells (Fig. 1B). The entry of NPN into the bacterial cell membranes was considered as a signature of the permeabilization of the outer membrane mediated by the cationic AMPs, as termed 'self-promoted' uptake process [56]. Taken together, cytokine release and NPN fluorescence experiments demonstrated that CDT efficiently neutralizes toxicity of LPS and also disrupts integrity of the outer-membrane.

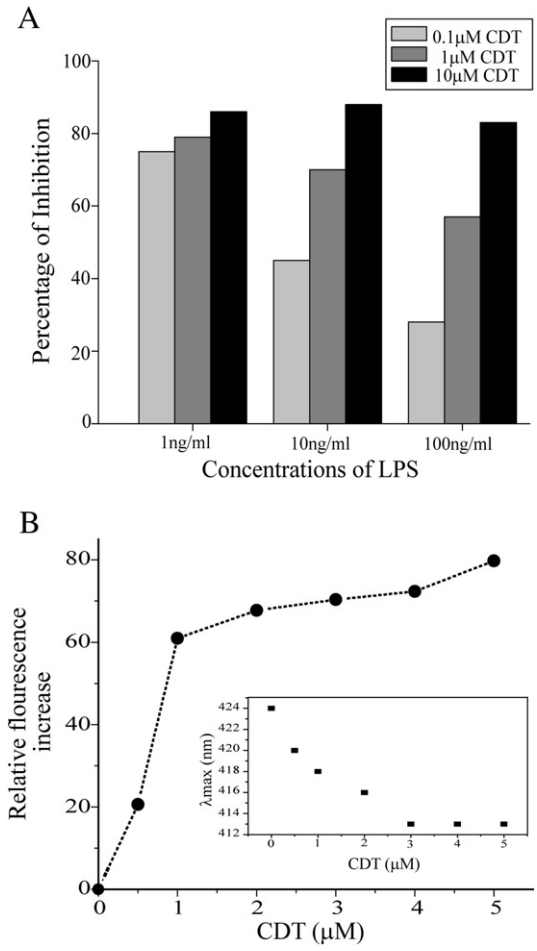

Fig. 1. LPS neutralization and outer membrane permeabilization by CDT. (panel A) Bar diagram showing inhibition of TNF-α secretion from macrophage stimulated with LPS in the presence of CDT peptide. Experiments were carried out with three different concentrations of LPS and three different concentrations of CDT. The percentage inhibition of TNF-α release by CDT was normalized with macrophage stimulated without peptide. As seen, CDT efficiently reduces TNF-α release by inhibiting LPS binding to macrophage cells. (panel B) Plot showing permeabilization of outer membrane of *E. coli* cells to the hydrophobic dye NPN as a function of concentration of CDT peptide. NPN showed an enhancement in fluorescence emission intensity and a blue shift in emission maxima (inset panel B) upon addition of CDT. The % membrane permeabilization was estimated with reference to polymyxin B.

3.2. Surface charge neutralization of *E. coli* cells by CDT

Zeta potential was measured for *E. coli* cells and LUV composed of POPC and LPS at various concentrations of CDT (Fig. 2). A negative zeta potential ~−20 mV was observed for the solutions of *E. coli* cells (Fig. 2). The LPS-outer membrane of *E. coli* is known to be contributing for the negative zeta potential [57,58]. Additions of CDT peptide caused a dramatic increase in zeta potential of *E. coli* cells (Fig. 2). Zeta potential was changed from −20 mV to 0 mV only at the 2 μM concentration of peptide (Fig. 2A). At the higher peptide concentrations (>2 μM) positive values of zeta potential were detected (Fig. 2). An analogous observation was also made for the zeta potential for mixed lipid vesicles containing zwitterionic lipid POPC and negatively charged LPS (Fig. 2). The neutralization of the surface charge (0 mV zeta potential) of the LPS-outer membrane by CDT can largely be accounted for a balance in electrostatic

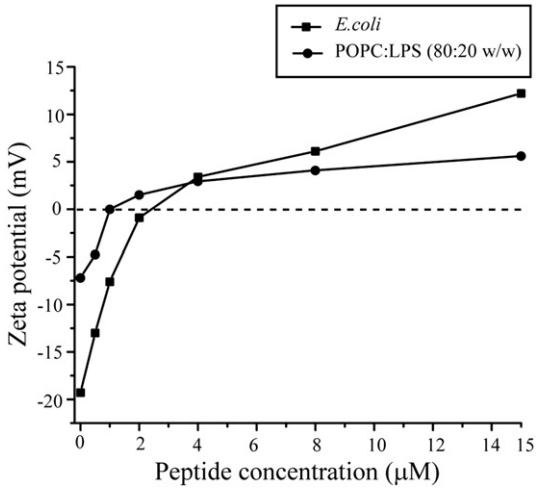

Fig. 2. Effect of CDT to the surface charge of *E. coli* and LUV: plot showing changes in zeta potential of *E. coli* cells and LUV of POPC-LPS (80:20 w/w) upon additions of CDT peptide. The dotted line at 0 mV zeta potential indicates an electrically neutral surface of *E. coli* and LUV obtained at 2 μM and 1 μM peptide concentrations, respectively.

interactions among the cationic residues of CDT with the negatively charged LPS lipids. However, the positive zeta potential, observed at >2 μM concentration of CDT, of *E. coli* cells may be interpreted as insertion of the peptide into the hydrophobic milieu of the LPS-outer membrane membranes [57,58]. These data demonstrated that as a mode of action CDT efficiently neutralizes surface charges of the outer membrane of *E. coli* cells and inserts into the hydrophobic environment of lipids.

3.3. Localization of Trp residue of CDT in LPS micelle

CDT contains a single Trp residue at position 2 in the amino acid sequence. The interactions between CDT and LPS were probed by means of intrinsic Trp emission and quenching experiments. In the free solutions, Trp residue of CDT showed an emission maximum at ~355 nm, indicating that Trp is highly solvent exposed (Fig. 3A). Inclusion of LPS at various concentrations into solutions containing CDT yielded a marked enhancement in the fluorescence emission intensity of Trp residue along with a blue shift in the emission maximum (Fig. 3A). At a 10 μM of LPS concentration, Trp residue of the peptide had an emission maximum of ~345 nm (Fig. 3A). These observations delineated the incorporation of Trp residue of CDT into the hydrophobic environment of LPS micelles. The extent of solvent accessibility of Trp was further determined by fluorescence quenching using acrylamide as a quencher. There was a limited quenching of Trp of CDT in complex with LPS in comparison to the free peptide (Fig. 3B). The Stern–Volmer quenching plots estimated a quenching constant (K_{sv}) of 20.0 and 8.4 for free and LPS-bound CDT, respectively (Fig. 3B). Collectively, fluorescence studies established that Trp residue of CDT is inserted into the non-polar milieu of the LPS lipid micelles with a restricted exposure to the aqueous solvent.

3.4. Secondary structures of CDT in LPS micelle

The global secondary structures of CDT were examined by CD and IR spectroscopic methods. Fig. 4A shows far UV CD spectra of CDT in free solution and in the presence of 50 μM LPS. The far UV CD spectra of CDT in buffer solutions were characterized by an intense single negative band at 200 nm, indicating random conformations of the peptide (Fig. 4A). By contrast, the far UV CD spectra of CDT obtained in a solution containing LPS micelles were dominated by the presence of two bands, with negative ellipticity, at 215 nm and 202 nm, implying structural transitions (Fig. 4A). The CD band detected at the wavelength at 215 nm could be interpreted in terms of populated β-sheet like structures of CDT in LPS micelles. Note that the estimation of secondary structures from CD spectra appeared to be complicated by the potential contribution to the far UV CD bands from the number of aromatic residues in CDT. A more definitive assignment of secondary structures of CDT in LPS micelles was further obtained from FT-IR studies. The secondary structure of CDT was determined following previous assignments in the amide I [59]. The spectra in the amide I region of CDT is shown after the subtraction of the LPS contribution

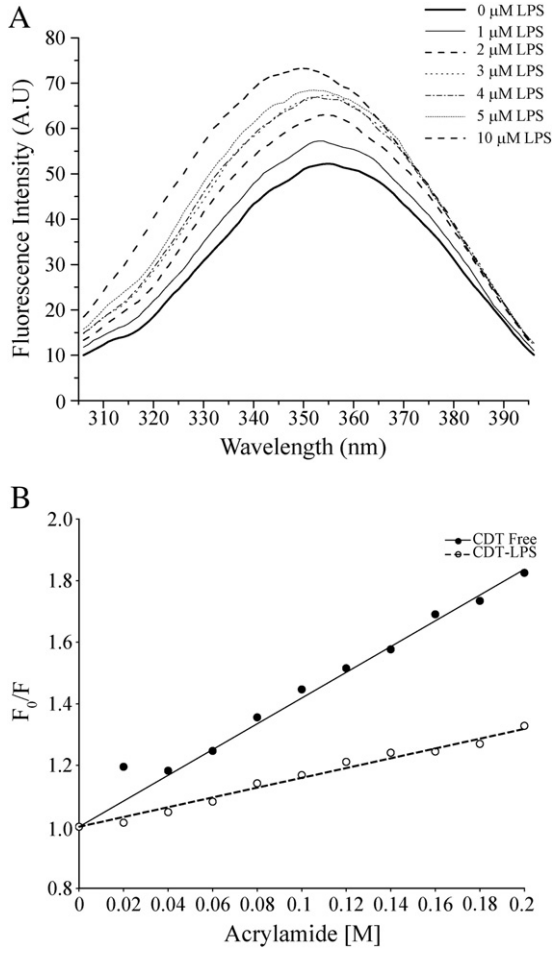

Fig. 3. Trp fluorescence emission and quenching of CDT. (panel A) Fluorescence emission spectra of Trp residue of CDT at different concentrations of LPS. (panel B) Plot showing a comparison of quenching of Trp fluorescence by acrylamide. Trp experienced both a blue shift in emission maxima (panel A) and a limited acrylamide quenching in the presence of LPS (panel B).

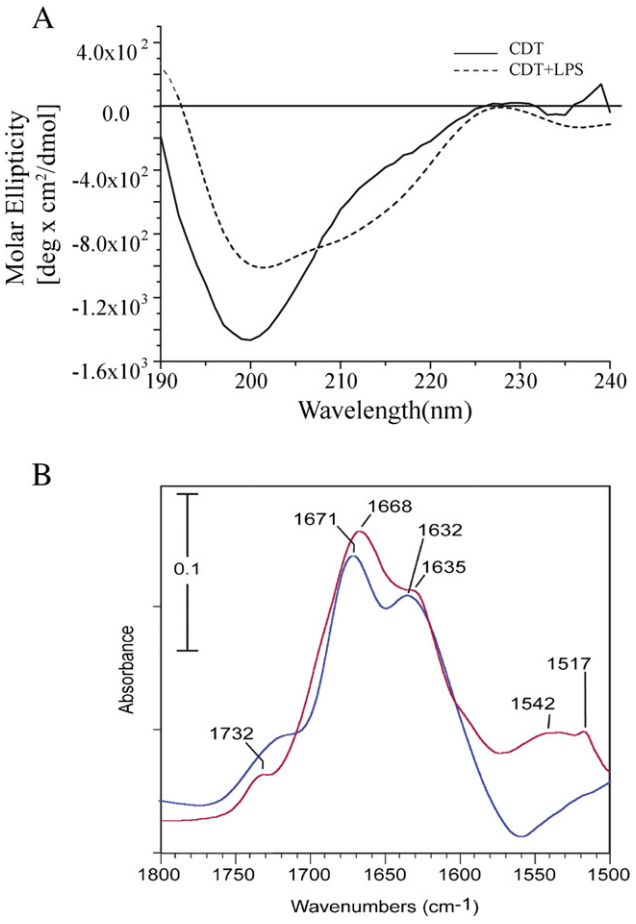

Fig. 4. Secondary structure of CDT in LPS by CD and IR spectroscopy: (panel A) far-UV CD spectra of CDT in the absence (solid line) and presence (dashed line) of 50 μM LPS. (panel B) Amide I and II regions corresponding to peptide CDT mixed with LPS in the presence of H_2O (red) and D_2O (blue). The wavenumbers (in cm^{-1}) of the main bands of both spectra are indicated.

in the presence of either H_2O or D_2O (Fig. 4B). The main bands in the spectrum in H_2O were centered at 1668 and 1635 cm^{-1}. The former band is indicative of β-turns or β-structures [59], whereas the band at 1635 cm^{-1} originates solely from β-structures. In any case, none of these bands can be assigned to α-helical structures or to random coils. The amide II band is visible at 1542 cm^{-1}, whereas the band at 1517 cm^{-1} corresponds to the tyrosine side chain of the peptide. After D_2O exchange (blue spectrum), the amide II appears to be completely shifted to lower wave numbers, which indicates a complete exchange (Fig. 4B). In the amide I, there was a small shift, from 1668 to 1671 cm^{-1}, and from 1635 to 1632 cm^{-1}. Due to the uncertainty in the assignment of the high frequency band, it is difficult to estimate the secondary structure composition, but one can refer to two limit situations; if the assignment of the 1668 cm^{-1} band corresponds to β-structure, then the peptide has 100% β-structure in LPS. If this band is assigned to β-turns, these would represent 58 ± 8% of the peptide, whereas 42 ± 12% is β-structure. These results apply regardless of the level of hydration: in the IR spectrum obtained in H_2O, bulk water was removed by nitrogen, whereas the sample in D_2O was hydrated in the ATR conditions. Yet, in these two conditions the amide I spectra appeared similar, except for small shifts due to H/D exchange.

3.5. Interactions of CDT and LPS by ITC

The binding affinity and thermodynamic parameters of interactions of CDT with LPS were quantified by use of ITC measurements. Fig. 5 shows a representative thermogram (at top) and integrated heats of binding between CDT and LPS (bottom) at 25 °C. As can be seen, LPS-peptide complex formation is driven by an endothermic reaction as indicated by an upward trend of the ITC peaks and a positive integrated heat (Fig. 5). An endothermic binding signifies a predominant role of hydrophobic interactions in the LPS–peptide complex formation. Note that interactions between AMPs and LPS have been found to be endothermic in nature at 25 °C or at lower temperatures, however, at higher temperatures (≥40 °C) exothermic binding to LPS was observed for some peptides [29,60,61]. This behavior has been rationalized in terms of phase transitions, gel phase (at 20 °C) to liquid crystalline phase (40 °C), of LPS lipids [60]. The equilibrium association constant (K_a) of interactions between CDT and LPS has been estimated to be 8.23 μM^{-1} (Table 1). All other thermodynamic parameters, ΔG, ΔH and TΔS, are listed in Table 1. The favorable change of free energy (ΔG) of interactions has been largely accounted by the positive change of entropy TΔS, as evident from the endothermic driven binding process (Table 1).

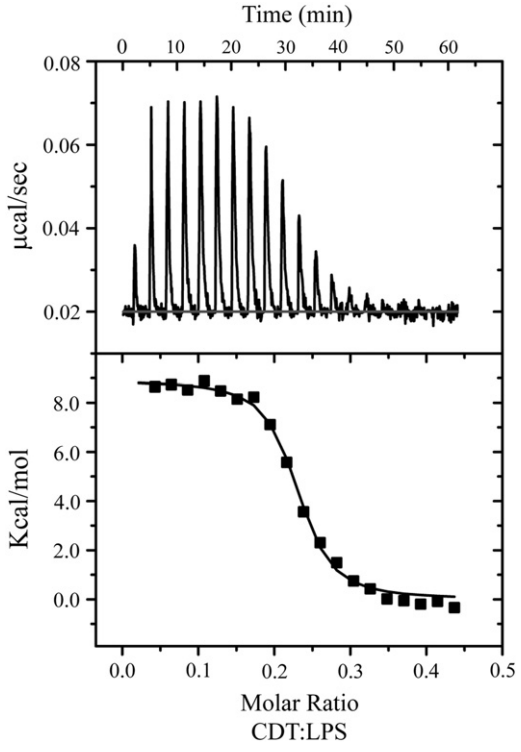

Fig. 5. Interactions between LPS and CDT by ITC. ITC measurement of 550 μM CDT titrated into 50 μM *E. coli* LPS in 10 mM sodium phosphate, pH 6.0 is shown at 298 K. The upper panel shows the ITC peaks plotted as power (μcal s^{-1}) against time (min). The lower panel shows the resulting integrated heats of the binding. ITC parameters are listed in Table 1.

3.6. NMR characterization of CDT in LPS micelles

Sequence-specific resonance assignment of CDT in free solution was made using two-dimensional ^1H–^1H TOCSY and NOESY spectra (Supplementary Fig. S1) [62]. In the free-state, the NOESY spectra of CDT were predominantly characterized by the sequential and intra-residue NOEs, indicating random conformations (Supplementary Fig. S2). Additions of low concentrations of LPS into solution containing CDT had resulted in broadening of NMR resonances, indicating a fast exchange between free and LPS-bound states of the peptide at NMR time scale (data not shown). Under such fast exchange regime, peptides may generate NOEs corresponding to the LPS-bound states that are detected in the NOESY spectra, also termed tr-NOESY [63,64], correlating resonances of the free peptides. tr-NOESY experiment is typically utilized to determine conformations of ligands, with a dissociation constant (K_d) of the mM–μM range, while bound to a high-molecular weight receptor [63,64]. It may be noted that LPS forms high molecular weight micelles at a significantly low concentration, 1 to 2 μM, than any other lipids [65], permitting observation of tr-NOEs from LPS-bound peptides [19,27–30]. As such, tr-NOESY has been the only method for the determination of atomic resolution structures of AMPs and LPS binding peptides in LPS micelle [27–30].

tr-NEOSY spectra of CDT obtained in the presence of 10 μM of LPS (see Materials and methods) revealed a large number of NOE contacts among the backbone–backbone, backbone–sidechain and sidechain–sidechain proton resonances. Fig. 6A shows a section of the tr-NOESY spectrum correlating NOEs among downfield shifted amide and aromatic proton resonances (7.5–8.5 ppm) with the upfield shifted aliphatic proton resonances (0.9–4.6 ppm). Further, the indole sidechain ($N^{\varepsilon}H$) proton of residue W2, at 10.1 ppm, delineated several NOEs with the aliphatic sidechain protons (Fig. 6B). By contrast, there was a lack of NOEs for indole sidechain ($N^{\varepsilon}H$) proton for the free peptide (Fig. 6 C). Analyses of tr-NEOSY spectra demonstrated preponderance of sequential, medium-range and long-range NOE contact for CDT in LPS micelle (Supplementary Fig. S3 and Table S1). Noticeably, there were a number of long-range NOEs among residues W2/I9, W2/R11, F3/R13, V5/R11, V5/R12 and R4/R14 of CDT in LPS micelle (Table S1). Fig. 7 summarizes the type and number of NOEs observed for CDT in LPS micelle. As can be seen, the residues W2, F3, R4 and V5 at the N-terminus and residues I9, R11, R12 and R13 at the C-terminus of CDT are involved in long-range NOE interactions in the presence of LPS micelles (Fig. 7). By contrast, residues, Y6 — G8, at the middle of the sequence were primarily characterized by the short-range NOEs (Fig. 7).

3.7. Three-dimensional structure of CDT in LPS micelle

An ensemble of structures of CDT, in complex with LPS micelles, was derived based on 139 NOE driven distance constraints including 19 medium-range and 25 long-range NOEs (Table 2). Fig. 8A shows a superposition of all backbone atoms (C^{α}, N, and C′) of the twenty lowest energy structures of CDT in LPS micelle. The RMSD values for backbone and heavy atoms from the mean structure were estimated

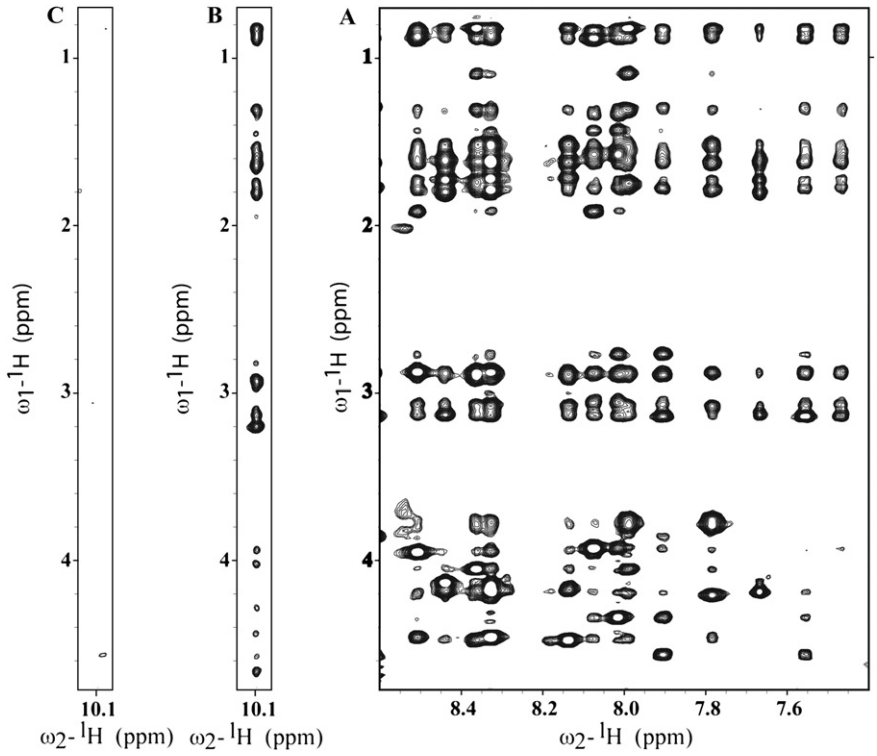

Fig. 6. 2D ^{1}H–^{1}H tr-NOESY spectra of CDT in LPS micelles. (panel A) A selected section of ^{1}H–^{1}H 2D tr-NOESY spectrum of CDT obtained in the presence of LPS micelles showing NOE correlations from downfield shifted aromatic and amide proton resonances (ω_2 dimension) with upfield shifted aliphatic proton resonances (ω_1 dimension). A comparison of NOE connectivities correlating the most downfield shifted N$^{\varepsilon}$H proton resonance ~10.1 ppm of residue Trp2 with aliphatic proton resonances of CDT in LPS micelles (panel B) and in free solution (panel C).

to be 0.08 ± 0.04 Å and 1.58 ± 0.26 Å, respectively (Table 2). The LPS-bound structure of CDT is characterized by a type II′ β-turn for the amino acid residues Y6 (i)–R7(i + 1)–G8(i + 2)–I9(i + 3) (Fig. 8B). The stereochemistry of the type II′ β-turn is maintained by a positive backbone ϕ dihedral angle for residue G8 located at the i + 2 position in the turn (Fig. 8B). In addition, the carboxyl oxygen (C═O) atom of residue Y6 has been found to be in close proximity with the amide hydrogen (NH) atom of residue I9, indicating the existence of a potential hydrogen bonding at the β-turn region. The residues W2–V5 and Y10–R13 at the N- and C-termini, respectively, assume extended or β-strand conformations. The two β-strands of CDT maintain an anti-parallel orientation through packing interactions among sidechains of aromatic and aliphatic amino acid residues (Fig. 8B and C). Notably, the indole ring of residue W2 shows van der Waals' packing interactions with the non-polar residues V5 and I9 (Fig. 8B). Further, the sidechain of residue W2 is also in a close proximity with the cationic sidechain of residue R11, plausibly indicating the involvement of cation–π interactions (Fig. 8B and C). The overall structure of CDT in LPS micelles resembles a β-hairpin topology. The β-hairpin structure of CDT deduced in LPS micelles is largely amphipathic with an aromatic and non-polar surface comprised by residues W2, F3, V5, Y6 and I9 and a positively charged surface made of cationic residues R4, R7, R12 and R13 (Fig. 8C and D). At the cationic surface of CDT, the guanidinium sidechain of residue R7, from the β-turn, and guanidinium sidechains of residues R12 and R13, from the C-terminal strand, are found to be separated with an average distance of 14 Å–15 Å (Fig. 8E). Note that such a distance is geometrically similar to the inter-phosphate distance of the lipid A moiety of LPS [19]. This observation may indicate that preferential ionic interactions may occur between the positively charged sidechains of residues R7, R12 and R13 with the phosphate groups of di-glucosamine of lipid A domain of LPS.

Table 1
Binding parameters obtained for CDT–LPS interactions in 10 mM sodium phosphate buffer with pH 6 at 20 °C by ITC experiments.

K_a (μM)	K_d (μM^{-1})	ΔH (kcal/mol)	ΔG (kcal/mol)	TΔS (kcal/mol)
8.23 ± 1.32	0.12 ± 0.4	8.9 ± 0.24	−6.0	14.9

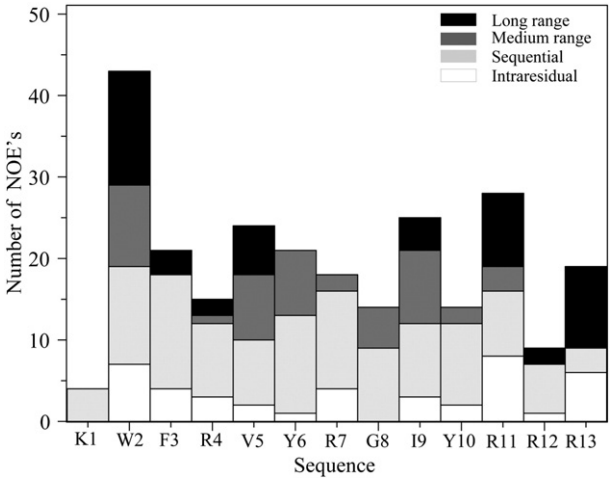

Fig. 7. Distribution of NOEs of CDT in LPS micelles: bar diagram summarizing NOE contacts detected for each amino acid residue of CDT in the complex with LPS micelles. As can be seen residue Trp2 yielded as many as 45 NOE interactions including a number of long-range NOEs.

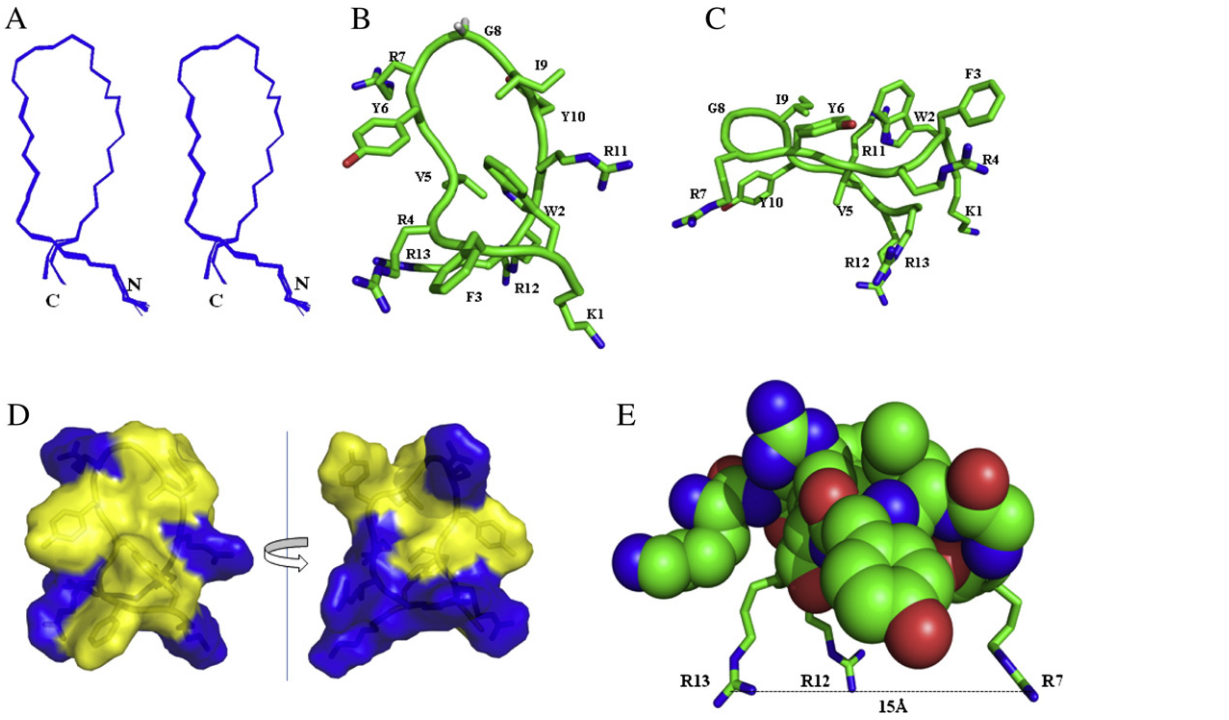

Fig. 8. Description of the 3-D structure of CDT in LPS micelles: (panel A) superposition of backbone atoms (N, C^{α}, C′) of the twenty lowest energy structures (in stereo) of CDT bound to LPS, obtained from CYANA 2.1. (panel B) A representative structure of CDT in LPS micelles showing β-hairpin like topology and sidechain orientation. (panel C) The β-hairpin like structure of CDT showing amphipathic segregation of amino acid residues. (panel D) Electrostatic surface potential of CDT structure in LPS micelles in two different orientations. (panel E) The polar or cationic face of the β-hairpin structure of CDT delineating a distance of ~15 Å between the nitrogen atoms of the sidechain guanidinium group of residues R13 and R7. This distance would be geometrically compatible with the inter-phosphate distance of the lipid A moiety of LPS.

3.8. Localization of CDT within LPS micelle by saturation transfer difference (STD) NMR

STD-NMR has been utilized to elucidate residues of AMPs in close proximity with LPS micelle [27,28,49,50]. The one-dimensional STD spectra of CDT demonstrated strong STD effects particularly for the aromatic and aliphatic sidechain proton resonances of CDT with LPS micelles, indicating an intimate association of the entire peptide with LPS micelle (Supplementary Fig. S4). By use of 2-D STD-TOSCY, residue-resolved interactions of CDT with LPS micelles were further achieved. Fig. 9 shows selected sections of the STD-TOCSY spectra showing correlations among the aliphatic proton resonances (panel A) and that of for the downfield shifted aromatic ring proton resonances (panel B). The STD-TOCSY spectra were interpreted based on the previous studies whereby resonances delineating cross-peaks are considered to be arising from the close contact of those residues with LPS micelle [29,50]. In the STD-TOCSY spectra, $C^{\alpha}H$ proton resonances of residues V5 and I9 showed correlations with the respective sidechain resonances (Fig. 9A). In addition, intense STD-TOCSY cross-peaks can be seen among the sidechain resonances of the residues V5 and I9 (Fig. 9A). These observations indicated that the backbone and the sidechain protons of V5 and I9 of CDT are in close proximity with the LPS micelles. By contrast, none of the aromatic residues, W2, F3, Y7 and Y10, of CDT exhibited cross-peaks between the $C^{\alpha}H$ and $C^{\beta}H$ resonances in the STD-TOCSY spectra, indicating their limited contact with the LPS micelle. The backbone $C^{\alpha}Hs$ of arginine residues, R4, R7, R11 and R13, either showed no cross-peaks or weaker cross-peaks with the sidechain $C^{\beta}Hs$, $C^{\gamma}Hs$ and $C^{\delta}Hs$ proton resonances, implying restricted contacts with the LPS molecules (Fig. 9A). However, the sidechain moieties of aromatic and cationic arginine residues of CDT demarcated a close proximity with the LPS micelle. There were strong cross-peaks observed in the STD-TOCSY spectra correlating ring proton resonances of aromatic residues W2, F3 and Y6/Y10 of CDT (Fig. 9B). Furthermore, the sidechain resonances of the arginine residues exhibited strong cross-peaks, clearly seen between the $C^{\delta}Hs$ resonating around 3.0 ppm to 3.2 ppm with the $C^{\beta}Hs$ and $C^{\gamma}Hs$ (Fig. 9A). Taken together, STD-TOCSY studies demonstrated that CDT has been effectively inserted within the LPS micelle predominantly employing sidechains of aromatic, aliphatic and cationic residues. However, the backbone region of the structure, except for V5 and I9, appears to contain only limited insertion within the LPS micelle.

Table 2
Summary of structural statistics of the twenty lowest energy structures of CDT bound to LPS micelles.

Distance restraints	
Intra-residue (|i − j| = 0)	39
Sequential (|i − j| = 1)	56
Medium range (2 ≤ |i − j| ≤ 4)	19
Long-range (|i − j| 5)	25
Total NOE constraints	139
Dihedral angle constraints (Φ)	12
Constraints violations	
Min NOE violation (Å)	0.09
Max NOE violation (Å)	0.26
Deviation from mean structure	
Backbone atoms (N, C^{α}, C′) (Å)	0.08 ± 0.04
Heavy atoms (Å)	1.58 ± 0.26
Ramachandran plot analysis	
% residues in the most favorable region	75.5
% residues additionally allowed region	24.5
% residues in the generously allowed region	0
% residues in the disallowed region	0

3.9. Perturbation of LPS micelles by CDT peptide

Interactions of AMPs with LPS have been observed to cause disorganization of the micelle structure of LPS [66,67]. We utilized FITC

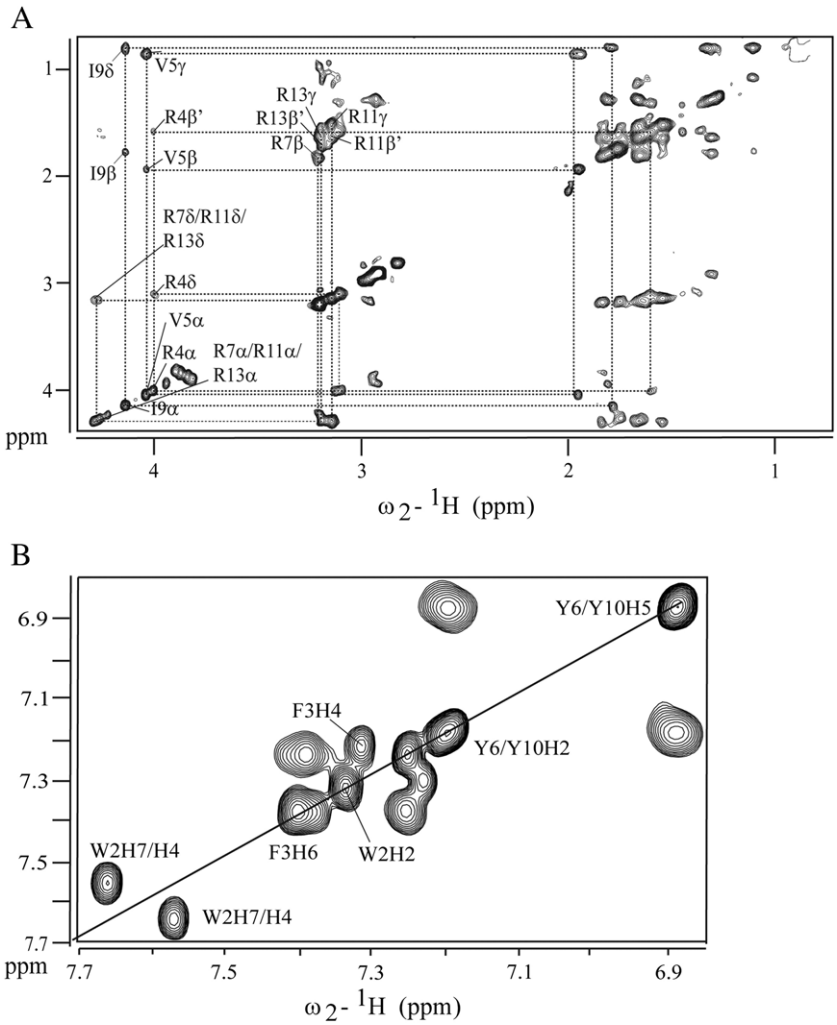

Fig. 9. Localization of CDT in LPS micelles by STD NMR: (panel A) STD-TOCSY spectrum of CDT presence of LPS showing correlations among aliphatic proton resonances. Through bond connectivities detected in STD-TOCSY spectra for amino acid residues of CDT are shown by broken lines. (panel B) STD-TOCSY spectrum of CDT presence in LPS showing correlations among aromatic proton resonances. STD-TOCSY spectra were acquired in D_2O using a spin-lock MLEV17 sequence with a mixing time of 80 ms.

fluorescence of FITC conjugated LPS (FITC-LPS) and dynamic light scattering (DLS) experiments probing plausible changes of LPS upon binding to CDT peptide. The intensity of FITC fluorescence emission of FITC-LPS is largely quenched due to the self association of LPS molecules. Additions of CDT peptide into solution containing FITC-LPS had produced a significant enhancement of the emission intensity of FITC fluorescence (Fig. 10A). The dequenching of FITC fluorescence of FITC-LPS demonstrated that binding of CDT to LPS micelles induces a dissociation of LPS aggregates. The dissociation of LPS micelles into smaller size aggregates can also be seen from DLS studies. In the absence of CDT peptide, LPS showed particle sizes with diameter centered at 5000 nm (Fig. 10B). There was a large shift in the distribution of LPS aggregate sizes in the presence of CDT peptide, whereby populations of LPS aggregates having smaller sizes, with diameter of 500 nm, became apparent upon addition of CDT peptide (Fig. 10C). Thus, FITC fluorescence and DLS data established that CDT peptide is able to impart perturbation of structural organizations of LPS micelles.

4. Discussion

The disulfide bonded β-hairpin structures of AMPs like TP-1, protegrins and polyphemusin exhibited a high correlation with antipathogenic activity [42–44,68,69]. In particular, linear analogs of TP-1 either with reduced disulfide bonds or Cys mutated to Ala showed lack of β-hairpin structure and markedly attenuated anti-bacterial activity [40–42,44]. In this regard, NMR techniques, both solution and solid, have been vital in determining atomic resolution structures, localization and structure–activity correlations of AMPs in a variety of model lipid membranes [15,18,19]. It may be interesting that the CDT peptide, despite the absence of disulfide bridges or complementary aromatic packing interactions, has retained β-hairpin like structure in complex with LPS micelle (Fig. 8). The β-hairpin structure of TP-I ($KWCFR^5VCYRG^{10}ICYRR^{15}CR\text{-}NH_2$) is well characterized by a β-turn for the centrally located residues Y–R–G–I [36,40]. As seen, the β-turn is even now preserved for these residues, Y6–R–G–I9, in the LPS-bound structure of CDT (Fig. 8B). The β-hairpin topology of CDT, stabilized in LPS micelles, is sustained by the unique packing interactions between the aromatic ring of W2 and the sidechain of non-polar amino acids of V5 and the cationic sidechain of residue R11 (Fig. 8B). There is also a close proximity between residues W2 and I9, supported by the NOEs involving indole ring protons of W2 with sidechain protons of I9 (Table S1). These packing interactions have rendered an approximate anti-parallel orientation of the hairpin structure of CDT in LPS. The 'flipping' of the bulky indole ring of W2 toward the residues of the β-turn has created a twist for the anti-parallel strands (Fig. 8B). On the other hand, the β-hairpin structure of TP-1 has been found to be rigid as a result of disulfide bridges and inter-strand packing interactions [42,43]. The 3-D structure and interactions of CDT with LPS micelle may provide mechanistic insights toward outer membrane permeabilization and endotoxin neutralization. The

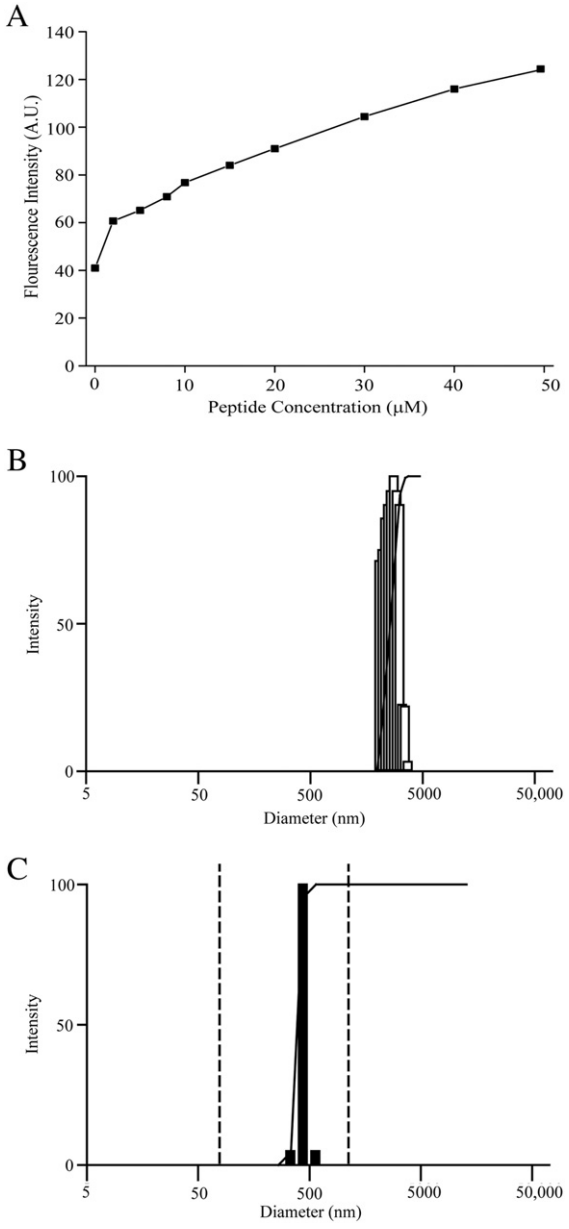

Fig. 10. Perturbations of LPS micelles by CDT. (panel A) Disaggregation of FITC labeled LPS by CDT using FITC fluorescence. The fluorescence intensity of FITC increases as a function of increasing concentrations of CDT peptide. Fluorescence studies were performed in 10 mM sodium phosphate buffer, pH 6.0 at 298 K. (panels B and C) Particle size measurements of LPS in free (panel B) and in the presence of CDT (panel C) from quasi elastic light scattering measurements. The average size of aggregates of LPS (panel B) is observed to decrease upon addition of CDT in a 1:2 molar ratio (panel C). Experiments were carried out in 10 mM sodium phosphate buffer, pH 6.0 at 298 K.

β-hairpin like structure of CDT displays an extended positively charged surface patch of residues R4, R7, R12 and R13 (Fig. 8D). As expected, these basic residues would be interacting, salt bridges and/or hydrogen bonds, with the anionic phosphate groups of LPS, as revealed from zeta potential experiments (Fig. 2). STD-NMR studies established a close proximity of the cationic sidechains of Arg residues with LPS micelle (Fig. 9). To obtain a molecular model of LPS–CDT interactions, the β-hairpin structure of CDT was iteratively docked with the lipid A moiety of LPS (Fig. 11). In particular, the guanidinium group of residue R7 of CDT is in close proximity to the phosphate group located at the O_4' position of glucosamine II, whereas the di-phosphate at the O1 position of glucosamine I can potentially form a number of salt-bridge interactions with residues R12 and R13 (Fig. 11). The guanidinium sidechain of R4 is also likely to be involved in a long-range ionic interaction with the di-phosphate groups of glucosamine I (Fig. 11). Notably, the guanidinium groups of R7 and R12/R13 in the β-hairpin structure of CDT maintain an inter-sidechain distance of ~15 Å closely matching the inter-phosphate distance, of 13 Å, between the O1 and O4 phosphate groups of lipid A (Fig. 8E). The amphipathic structure of CDT demarcates a hydrophobic surface consisted of residues W2, F3, Y6, I9 and Y10 (Fig. 8). The basic residue R11 also resides at the hydrophobic face as a result of close packing with the indole ring of W2 (Fig. 8). STD-NMR reveals involvement of these aromatic and aliphatic residues including R11, through the sidechain moieties, in LPS binding (Fig. 9). The model of LPS–CDT complex shows that the hydrophobic surface of the structure of CDT can insert along the acyl chains of the LPS lipids (Fig. 11). As seen, the blue shift in the emission maximum of Trp and a limited quenching by acrylamide indicated a plausible inclusion of the fluorophore into the hydrophobic core of LPS micelle (Fig. 3). The positively charged sidechain of R11 can be favorably placed at the hydrophobic milieu of LPS (Fig. 11) as a consequence of the interactions, cation–π type, with an indole ring of W2 [70]. Such cationic–π interactions, specifically between Arg and Trp, have been proposed to shield the charge and may allow a deeper penetration of the AMPs inside the hydrophobic environment of lipid bilayer structure [71,72]. Insertion of CDT within the LPS micelle leads to significant perturbation of the LPS packing organization. The enhanced fluorescence of FITC-conjugated LPS and generation of smaller micelles of LPS observed upon addition of CDT peptide suggested diminution of interactions among LPS lipids (Fig. 10). Thus, these interactions between CDT and LPS may lead to a plausible disruption or fluidization of LPS structures facilitating

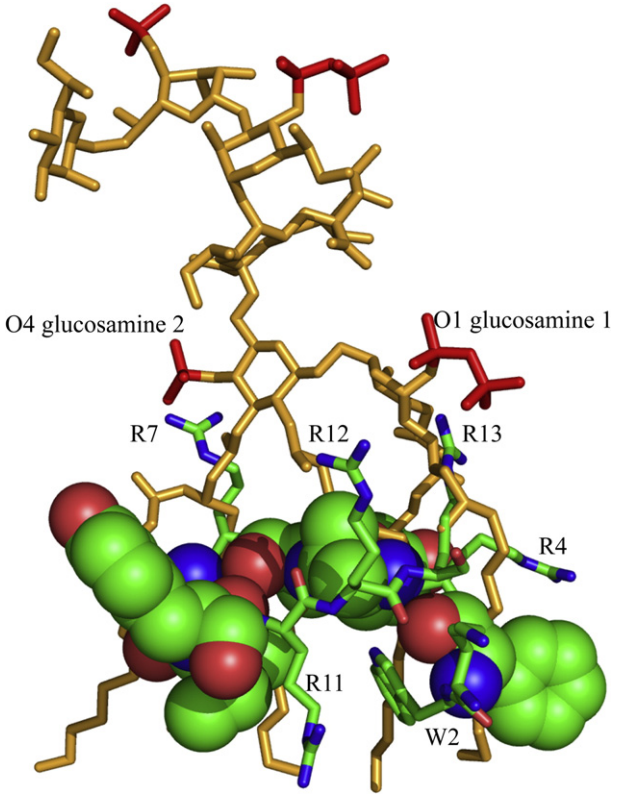

Fig. 11. Mode of interaction of CDT with LPS: a molecular model of CDT–LPS complex showing close proximity of the negatively charged phosphate groups of glucosamine 1 and glucosamine 2 of the lipid A moiety of LPS with the sidechains of cationic residues R7, R12 and R13. The sidechains of residues R11 and W4, with probable cation–π interactions, are rather deeply inserted, along with other aromatic and non-polar residues, to the hydrophobic acyl region of LPS. The image was produced using INSIGHTII.

traversal of the peptide through the LPS-outer membrane. The compact β-hairpin structure of CDT will certainly aid in the process of permeation through the outer membrane. In conclusion, we demonstrate that CDT, the Cys deleted analog TP-I, assumes a β-hairpin like unique three-dimensional structure, despite the absence of disulfide bonds, in complex with LPS micelles. It is noteworthy that this is the first structure of a host-defense AMP in the LPS micelle that belongs to the β-hairpin family. Thus far largely helical structures of AMPs had been reported in LPS lipids [28–30,47,73]. In addition, current study identifies important structural features of CDT for LPS recognition and provides a plausible mechanism of the outer membrane disruption. We believe that structure of CDT in LPS and other findings in this study may be utilized for the development of new antimicrobials, possibly with the incorporation of fluorinated amino acid analogs [74], with enhanced binding affinity for endotoxin.

Acknowledgements

This work was supported by grants RG49/10 and 08/1/22/19/556, from the Academic Research Fund, Tier 1, Ministry of Education, Singapore and A*Star Biomedical Research Council, Singapore. The atomic coordinates and NMR constraints of CDT have been deposited to the protein data bank (PDB: 21m8) and BMRB under the accession code 18102.

Appendix A. Supplementary data

Supplementary data to this article can be found online at doi:10.1016/j.bbamem.2012.03.015.

References

[1] J. Verhoef, Antibiotic resistance: the pandemic, Adv. Exp. Med. Biol. 531 (2003) 301–313.
[2] S.B. Levy, B. Marshall, Antibacterial resistance worldwide: causes, challenges and responses, Nat. Med. 10 (2004) S122–S129 (Suppl.).
[3] F.M. Walsh, S.G.B. Amyes, Microbiology and drug resistance mechanisms of fully resistant pathogens, Curr. Opin. Microbiol. 7 (2004) 439–444.
[4] R.A. Weinstein, Controlling antimicrobial resistance in hospitals: infection control and use of antibiotics, Emerg. Infect. Dis. 7 (2001) 188–192.
[5] G. Taubes, The bacteria fight back, Science 321 (2008) 356–361.
[6] R.E.W. Hancock, Peptide antibiotics, Lancet 349 (1997) 418–422.
[7] M. Zasloff, Antimicrobial peptides of multicellular organisms, Nature 415 (2002) 389–395.
[8] K.A. Brogden, Antimicrobial peptides: pore formers or metabolic inhibitors in bacteria? Nat. Rev. Microbiol. 3 (2005) 238–250.
[9] H. Jenssen, P. Hamill, R.E.W. Hancock, Peptide antimicrobial agents, Clin. Microbiol. Rev. 19 (2006) 491–511.
[10] V. Dhople, A. Krukemeyer, A. Ramamoorthy, The human beta-defensin-3, an antibacterial peptide with multiple biological functions, Biochim. Biophys. Acta 1758 (2006) 1499–1512.
[11] K.L. Brown, R.E.W. Hancock, Cationic host defense (antimicrobial) peptides, Curr. Opin. Immunol. 18 (2006) 24–30.
[12] R.M. Epand, H.J. Vogel, Diversity of antimicrobial peptides and their mechanisms of action, Biochim. Biophys. Acta 1462 (1999) 11–28.
[13] K. Matsuzaki, Magainins as paradigm for the mode of action of pore forming polypeptides, Biochim. Biophys. Acta 1376 (1998) 391–400.
[14] N. Papo, Y. Shai, Host defense peptides as new weapons in cancer treatment, Cell Mol. Life Sci. 62 (2005) 784–790.
[15] L.T. Nguyen, E.F. Haney, H.J. Vogel, The expanding scope of antimicrobial peptide structures and their modes of action, Trends Biotechnol. 29 (2011) 464–472.
[16] R.M. Epand, R.F. Epand, Bacterial membrane lipids in the action of antimicrobial agents, J. Pept. Sci. 17 (2011) 298–305.
[17] H. Nikaido, Molecular basis of bacterial outer membrane permeability revisited, Microbiol. Mol. Biol. Rev. 67 (2003) 593–656.
[18] A. Ramamoorthy, Beyond NMR spectra of antimicrobial peptides: dynamical images at atomic resolution and functional insights, Solid State Nucl. Magn. Reson. 35 (2009) 201–207.
[19] S. Bhattacharjya, A. Ramamoorthy, Multifunctional host defense peptides: functional and mechanistic insights from NMR structures of potent antimicrobial peptides, FEBS J. 276 (2009) 6465–6473.
[20] D.S. Snyder, T.J. McIntosh, The lipopolysaccharide barrier: correlation of antibiotic susceptibility with antibiotic permeability and fluorescent probe binding kinetics, Biochemistry 39 (2000) 11777–11787.
[21] L. Ding, L. Yang, T.M. Weiss, A.J. Waring, R.I. Lehrer, H.W. Huang, Interaction of antimicrobial peptides with lipopolysaccharides, Biochemistry 42 (2003) 12251–12259.
[22] H. Steiner, D. Hultmark, A. Engstrom, H. Bennich, H.G. Boman, Sequence and specificity of two antibacterial proteins involved in insect immunity, Nature 292 (1981) 246–248.
[23] M. Dante, T. Wieprecht, Structural features of helical antimicrobial peptides: their potential to modulate activity on model membranes and biological cells, Biochim. Biophys. Acta 1462 (1999) 71–87.
[24] Y. Rosenfeld, D. Barra, M. Simmaco, Y. Shai, M.L. Mangoni, A synergism between temporins toward Gram-negative bacteria overcomes resistance imposed by the lipopolysaccharide protective layer, J. Biol. Chem. 281 (2006) 28565–28574.
[25] M.L. Mangoni, Y. Shai, Temporins and their synergism against Gram-negative bacteria and in lipopolysaccharide detoxification, Biochim. Biophys. Acta 1788 (2009) 1610–1619.
[26] N. Papo, Y. Shai, A molecular mechanism for lipopolysaccharide protection of Gram-negative bacteria from antimicrobial peptides, J. Biol. Chem. 280 (2005) 10378–10387.
[27] S. Bhattacharjya, De novo designed lipopolysaccharide binding peptides: structure based development of antiendotoxic and antimicrobial drugs, Curr. Med. Chem. 17 (2010) 3080–3093.
[28] A. Bhunia, A. Ramamoorthy, S. Bhattacharjya, S. Helical, hairpin structure of a potent antimicrobial peptide MSI-594 in lipopolysaccharide micelles by NMR spectroscopy, Chemistry 15 (2009) 2036–2040.
[29] A. Bhunia, P. Domadia, J. Torres, K.J. Hallock, A. Ramamoorthy, S. Bhattacharjya, NMR structure of pardaxin, a pore-forming antimicrobial peptide, in lipopolysaccharide micelles: mechanism of outer membrane permeabilization, J. Biol. Chem. 285 (2010) 3883–3895.
[30] P. Domadia, A. Bhunia, A. Ramamoorthy, S. Bhattacharjya, Structure, interactions, and antibacterial activities of MSI-594 derived mutant peptide MSI-594F5A in lipopolysaccharide micelles: role of the helical hairpin conformation in outer-membrane permeabilization, J. Am. Chem. Soc. 132 (2010) 18417–18428.
[31] S. Bhattacharjya, P. Domadia, A. Bhunia, S. Malladi, S. David, High resolution solution structure of a designed peptide bound to lipopolysaccharide: transferred nuclear Overhauser effects, micelle selectivity and anti-endotoxic activity, Biochemistry 46 (2007) 5864–5874.
[32] S. Bhattacharjya, S. David, V. Mathan, P. Balaram, Polymyxin B nonapeptide: conformations in water and in lipopolysaccharide-bound state determined by 2-D NMR and molecular dynamics, Biopolymers 41 (1997) 251–265.
[33] G.S. Martin, D.M. Mannino, S. Eaton, M.N. Moss, The epidemiology of sepsis in the United States from 1979 through 2000, Engl. J. Med. 348 (2003) 1546–1554.
[34] D.C. Angus, R.S. Wax, Epidemiology of sepsis: an update, Crit. Care Med. 29 (2001) S109–S116.
[35] S.A. David, Towards a rational development of anti-endotoxin agents: novel approaches to sequestration of bacterial endotoxins with small molecules, J. Mol. Recognit. 6 (2011) 370–387.
[36] R. Jerala, M. Porro, Endotoxin neutralizing peptides, Curr. Top. Med. Chem. 4 (2004) 1173–1184.
[37] T. Nakamura, H. Furunaka, T. Miyata, F. Tokunaga, T. Muta, S. Iwanaga, M. Niwa, T. Takao, Y. Shimonishi, Tachyplesin, a class of antimicrobial peptide from the hemocytes of the horseshoe crab (*Tachypleus tridentatus*). Isolation and chemical structure, J. Biol. Chem. 263 (1988) 16709–16713.
[38] K. Kawano, T. Yoneya, T. Miyata, K. Yoshikawa, F. Tokunaga, Y. Terada, S. Iwanag, Antimicrobial peptide, tachyplesin I, isolated from hemocytes of the horseshoe crab (*Tachypleus tridentatus*). NMR determination of the beta-sheet structure, J. Biol. Chem. 265 (1990) 15365–15367.
[39] M. Ohta, H. Ito, K. Masuda, S. Tanaka, Y. Arakawa, R. Wacharotayankun, N. Kato, Mechanisms of antibacterial action of tachyplesins and polyphemusins, a group of antimicrobial peptides isolated from horseshoe crab hemocytes, Antimicrob. Agents Chemother. 36 (1992) 1460–1465.
[40] H. Tamamura, R. Ikoma, M. Niwa, S. Funakoshi, T. Murakami, N. Fujii, Antimicrobial activity and conformation of tachyplesin I and its analogs, Chem. Pharm. Bull. 41 (1993) 978–980.
[41] K. Matsuzaki, M. Fukui, N. Fujii, K. Miyajima, Interactions of an antimicrobial peptide, tachyplesin I, with lipid membranes, Biochim. Biophys. Acta 1070 (1991) 259–264.
[42] A. Laederach, A.H. Andreotti, D.B. Fulton, Solution and micelle-bound structures of tachyplesin I and its active aromatic linear derivatives, Biochemistry 41 (2002) 12359–12368.
[43] T. Doherty, A.J. Waring, M. Hong, Membrane-bound conformation and topology of the antimicrobial peptide tachyplesin I by solid-state NMR, Biochemistry 45 (2006) 13323–13330.
[44] A.G. Rao, Conformation and antimicrobial activity of linear derivatives of tachyplesin lacking disulfide bonds, Arch. Biochem. Biophys. 361 (1999) 127–134.
[45] J.P. Tam, Y.A. Lu, J.L. Yang, Marked increase in membranolytic selectivity of novel cyclic tachyplesins constrained with an antiparallel two-beta strand cystine knot framework, Biochem. Biophys. Res. Commun. 267 (2000) 783–790.
[46] K. Matsuzaki, S. Yoneyama, N. Fujii, K. Miyajima, K. Yamada, Y. Kirino, K. Anzai, Membrane permeabilization mechanisms of a cyclic antimicrobial peptide, tachyplesin I, and its linear analog, Biochemistry 36 (1997) 9799–9806.
[47] K.B. Chandrababu, B. Ho, D. Yang, Structure, dynamics, and activity of an all-cysteine mutated human beta defensin-3 peptide analogue, Biochemistry 48 (2009) 6052–6061.
[48] A. Ramamoorthy, S. Thennarasu, A. Tan, K. Gottipati, S. Sreekumar, D.L. Heyl, F.Y. An, C.E. Shelburne, Deletion of all cysteines in tachyplesin I abolishes hemolytic activity and retains antimicrobial activity and lipopolysaccharide selective binding, Biochemistry 45 (2006) 6529–6540.
[49] A. Bhunia, P.N. Domadia, S. Bhattacharjya, Structural and thermodynamic analyses of the interaction between melittin and lipopolysaccharide, Biochim. Biophys. Acta 1768 (2007) 3282–3291.

[50] A. Bhunia, S. Bhattacharjya, Mapping residue-specific contacts of polymyxin B with lipopolysaccharide by saturation transfer difference NMR: insights into outer-membrane disruption and endotoxin neutralization, Biopolymers (Peptide Sci.) 96 (2010) 273–287.
[51] P. Guntert, C. Mumenthaler, K. Wuthrich, Torsion angle dynamics for NMR structure calculation with the new program DYANA, J. Mol. Biol. 273 (1997) 283–298.
[52] R.A. Laskowski, J.A. Rullmannn, M.W. MacArthur, R. Kaptein, J.M. Thornton, AQUA and PROCHECK-NMR: programs for checking the quality of protein structures solved by NMR, J. Biomol. NMR 8 (1996) 477–486.
[53] Y.J. Huang, R. Powers, G.T. Montelione, Protein NMR recall, precision, and F-measure scores (RPF scores): structure quality assessment measures based on information retrieval statistics, J. Am. Chem. Soc. 127 (2005) 1665–1674.
[54] M.G. Scott, A.C. Vreugdenhil, W.A. Buurman, R.E.W. Hancock, M.R. Gold, Cutting edge: cationic antimicrobial peptides block the binding of lipopolysaccharide (LPS) to LPS binding protein, J. Immunol. 164 (2000) 549–553.
[55] B. Beutler, Tlr4: central component of the sole mammalian LPS sensor, Curr. Opin. Immunol. 12 (2000) 20–26.
[56] R.E.W. Hancock, Alterations in outer membrane permeability, Annu. Rev. Microbiol. 38 (1984) 237–264.
[57] C.S. Alves, M.N. Melo, H.G. Franquelim, R. Ferre, M. Planas, L. Feliu, E. Bardají, W. Kowalczyk, D. Andreu, N.C. Santos, M.X. Fernandes, M.A. Castanho, Escherichia coli cell surface perturbation and disruption induced by antimicrobial peptides BP100 and pepR, J. Biol. Chem. 285 (2010) 27536–27544.
[58] M.M. Domingues, M.A. Castanho, N.C. Santos, rBPI(21) promotes lipopolysaccharide aggregation and exerts its antimicrobial effects by (hemi)fusion of PG-containing membranes, PLoS One 4 (2009) e8385.
[59] D.M. Byler, H. Susi, Examination of the secondary structure of proteins by deconvolved FTIR spectra, Biopolymers 25 (1986) 469–487.
[60] J. Howe, J. Andrä, R. Conde, M. Iriarte, P. Garidel, M.H. Koch, T. Gutsmann, I. Moriyón, K. Brandenburg, Thermodynamic analysis of the lipopolysaccharide-dependent resistance of gram-negative bacteria against polymyxin B, Biophys. J. 92 (2007) 2796–2805.
[61] A. Bhunia, H. Mohanram, P.N. Domadia, J. Torres, S. Bhattacharjya, Designed beta-boomerang antiendotoxic and antimicrobial peptides: structures and activities in lipopolysaccharide, J. Biol. Chem. 284 (2009) 21991–22004.
[62] K. Wüthrich, NMR of Protein and Nucleic Acids, John Wiley & Sons, New York, 1986.
[63] G.M. Clore, A.M. Gronenborn, Theory and applications of the transferred nuclear Overhauser effect to the study of the conformations of small ligands bound to proteins, J. Magn. Reson. 48 (1982) 402–417.
[64] M. Mayer, B. Meyer, Characterization of ligand binding by saturation transfer difference NMR spectroscopy, Angew. Chem. Int. Ed. Engl. 38 (1999) 1784–1788.
[65] N.C. Santos, A.C. Silva, M.A. Castanho, J. Martins-Silva, C. Saldanha, Evaluation of lipopolysaccharide aggregation by light scattering spectroscopy, ChemBioChem 4 (2003) 96–100.
[66] P.S. Tobias, K. Soldau, J.A. Gegner, D. Mintz, R.J. Ulevitch, Lipopolysaccharide binding protein-mediated complexation of lipopolysaccharide with soluble CD14, J. Biol. Chem. 270 (1995) 10482–10488.
[67] Y. Rosenfeld, H.G. Sahl, Y. Shai, Parameters involved in antimicrobial and endotoxin detoxification activities of antimicrobial peptides, Biochemistry 47 (2008) 6468–6478.
[68] J.-P. Power, A. Tan, A. Ramamoorthy, R.E.W. Hancock, Solution structure and interactions of the antimicrobial polyphemusins with lipid membranes, Biochemistry 44 (2005) 15504–15513.
[69] L. Gottler, R. Bea, C. Shelburne, A. Ramamoorthy, E.N. Marsh, Using fluorous amino acids to probe the effects of changing hydrophobicity on the physical and biological properties of the β-hairpin antimicrobial peptide protegrins-1, Biochemistry 47 (2008) 9243–9250.
[70] D.I. Chan, E.J. Prenner, H.J. Vogel, Tryptophan- and arginine-rich antimicrobial peptides: structures and mechanisms of action, Biochim. Biophys. Acta 1758 (2006) 1184–1202.
[71] D.A. Dougherty, Cation–pi interactions in chemistry and biology: a new view of benzene, Phe Tyr Trp Sci. 271 (1996) 163–168.
[72] W. Jing, A.R. Demcoe, H.J. Vogel, Conformation of a bactericidal domain of puroindoline a: structure and mechanism of action of a 13-residue antimicrobial peptide, J. Bacteriol. 185 (2003) 4938–4947.
[73] A. Bhunia, R. Saravanan, H. Mohanram, M.L. Mangoni, S. Bhattacharjya, NMR structures and interactions of temporin-1Tl and temporin-1 Tb with lipopolysaccharide micelles: mechanistic insights into outer membrane permeabilization and synergistic activity, J. Biol. Chem. 286 (2011) 24394–24406.
[74] E.N. Marsh, B. Buer, A. Ramamoorthy, Fluorine—a new element in the design of membrane-active peptides, Mol. Biosyst. 5 (2009) 1143–1147.